INTERNATIONAL JOURNAL OF MECHANICS
DOI: 10.46300/9104.2026.20.1 Volume 20, 2026

Application of WASPAS Method to Find the Best Input Factors in Internal Grinding SKD11 Tool Steel

Vu Duc Binh[1], Le Duc Bao[2], Dinh Van Thanh[3], Luu Anh Tung[4], Nguyen Thanh Tu[4,*]
[1]Viet Tri University of Industry, Vietnam
[2]Ha Noi University of Science and Technology, Vietnam
[3]East Asia University of Technology, Vietnam
[4]Thai Nguyen University of Technology, Vietnam

**Corresponding Author*

Received: March 19, 2025. Revised: June 23, 2025. Accepted: July 15, 2025. Available online: December 19, 2025.

Abstract - The paper reports the results of an optimization study aimed at identifying the ideal input parameters for the internal grinding process of cylindrical-shaped SKD11 tool steel components. Initially, the MEREC method was employed to calculate the criterion weights. The Weighted Aggregates Sum Product Assessment (WASPAS) method was subsequently utilized to tackle the MCDM problem. Additionally, three objectives were examined: surface roughness (SR), material removal rate (MRR), and wheel life (Lw). Additionally, six input factors have been analyzed: rough dressing depth (a_r), rough dressing times (n_r), fine dressing depth (a_f), fine dressing times (n_f), non-feeding dressing (n_0), and dressing feed rate (S_d). The Taguchi method utilizing the L16 ($4^4 + 2^2$) design and the Minitab R19 software were employed to structure the experiment and analyze the results. The MCDM problem has been effectively addressed, and optimal process factors were found.

Keywords - Internal Grinding, MCDM, WASPAS, MEREC, Surface Roughness, Material Removal Rate, Wheel Life.

I. Introduction

So far, various studies have been undertaken to examine the grinding process. A research was executed to enhance the grinding process of nickel-based superalloy by addressing the issues of elevated grinding temperatures and reduced machining efficiency, [1]. This study presents the preparation of an internal cooling wheel (ICW) featuring abrasives arranged in a phyllotactic pattern, aimed at enhancing machined surface integrity and minimizing grinding temperatures. A finite element model of the grinding zone was developed to investigate the effects of grinding wheel size and abrasive arrangement on the heat transfer performance and flow characteristics of the grinding fluid within the grinding zone. The experimental results indicate that grinding with the new model can reduce grinding temperatures by more than 20% and decrease surface roughness values by over 30%. A novel technique for dressing diamond grinding wheels utilizing abrasive waterjet (AWJ) technology to mitigate workpiece damage and wheel clogging associated with grinding challenging materials using traditional diamond grinding wheels was proposed in [2]. The primary process parameters were established according to the theoretical model for treating diamond grinding wheels utilizing AWJ. Response surface methodology (RSM) and backpropagation artificial neural networks (BP-ANN) were utilized to develop regression models correlating process factors with microgroove features. A comparative analysis was conducted to assess the predictive efficacy of both RSM and BP-ANN. The findings demonstrated that both BP-ANN and RSM are effective methodologies for forecasting microgroove attributes. The results of a study on monitoring grinding wheel wear with internal control signals during the surface grinding of 100Cr6 were presented in [3]. The suggested model can predict tool life with a R^2 value of 0.98 and is applicable for monitoring grinding wheel wear. B. The design of a new grinding head designed to enhance grinding efficiency and the quality of machined surfaces has been introduced in [4]. The design of the grinding head involves an analysis and discussion of several characteristics, including the number of grooves, groove width, helix angle, and the effective grinding area ratio, and their impact on the grinding process. The validated experimental results indicate that the grinding force and surface roughness with the new grinding head are 73% and 10% lower than those with the conventional grinding head, respectively.

A mathematical model for the grinding force (GF) and grinding temperature (GT) of a single particle has been proposed in [5]. A numerical simulation was conducted to evaluate the interaction among grinding parameters, grinding force-thermal coupling, and the residual stress of a single

particle. Simultaneously, focusing on the multi-grain grinding of aircraft precision high-speed bearing rings, an experimental investigation was conducted on crystal fragmentation, elemental composition, and residual stress of both serviceable and non-serviceable bearing rings. The simulation yielded the following results: the residual stress in the Y direction exceeds that in the X direction, which in turn surpasses the residual stress in the Z direction, all under identical grinding force and temperature conditions. An examination into the impact of grinding wheel wear on cutting forces, and the topography of the grinding wheel is examined with the aim of establishing a characteristic that enables the quantification of grinding wheel wear in a non-destructive manner was reported in [6]. It was reported that, following a brief conditioning phase, cutting forces rise in a roughly linear manner with the machined length. During this second phase, the force ratio tends toward a constant value, and the predominant wear process is the formation of flat surfaces on the diamond grains. In these circumstances, the 3D surface roughness metrics Sa, Sq, Spk, and Sku have demonstrated efficacy in monitoring wheel wear. The influence of diverse process parameters, such as grinding orientations, mesh size of grinding heads, and rotational speed, on the grinding quality of Carbon Fiber Reinforced Polymers (CFRP) utilizing industrial robots was investigated in [7]. The mechanism of grinding flaws was examined as well. High-speed grinding enhances the surface quality of CFRP. It was noted that the utilization of diamond grinding heads with excessively fine or big particles may diminish surface quality. In addition, the quality of grinding varies with the direction of grinding.

The impact of speed on the development of machined surfaces during ultra-high-speed grinding of IN718 superalloy at velocities reaching 240 m/s was evaluated in [8]. This study meticulously analyzes grinding forces and surface integrity across several speed ranges. Various methodologies are utilized to characterize and investigate the subsurface microstructure. The findings indicate that brittle-mode removal of IN718 superalloy transpires at grinding speeds surpassing 190 m/s, hence successfully reducing work hardening and thermal generation caused by heightened plastic deformation. Moreover, the machining speed affects the formation mechanism of the recrystallization layer, progressively shifting from the dominance of discontinuous dynamic recrystallization (dDRX) to that of continuous dynamic recrystallization (cDRX) as grinding speed increases. An investigation into the surface roughness characteristics of the inner raceway of the outer ring of tapered roller bearings during the grinding process was conducted in [9]. A model was proposed in the study to predict grinding surface roughness. The model has been developed utilizing parameters of the grinding wheel and is founded on the conversion relationship between bearing raceway grinding and surface grinding, as well as the motion trajectory of particles on the grinding wheel surface. The model was verified through experiments utilizing the current industrial process parameters for grinding bearing raceways. In [10], a study focused on the prediction and optimization of the stability of a multi-regenerative weak stiffness grinding system was performed. This work utilizes microstructured tools designed to maintain system stability while preserving the material removal rate. The influence of microstructure patterns on the regeneration delay of workpieces and the delay in tool wear within a grinding system characterized by a large aspect ratio was analyzed. A multi-regeneration stability model is established based on a microstructure tool. The experimental results indicate that the established theoretical model can accurately predict the boundaries of grinding stability. An investigation into spindle precision bearings and thin-walled bearings for rotary vector (RV) reducers has been conducted in [11]. The influence of grinding force, grinding temperature, grinding strain, grinding vibration, and grinding acoustic emission on the metamorphic layer of bearings and the surface topography of workpieces has been analyzed. The analysis indicates that feed speed exerts the most significant impact on grinding force and wheel speed. Additionally, grinding depth significantly affects grinding temperature, while wheel speed has the most substantial impact on grinding strain and feed speed.

An investigation into the development of the surface-affected layer during the grinding of ultra-high strength steel was performed in [12]. This study utilized both simulation and experimental methods to investigate the grinding force, grinding temperature field, stress field, strain field, residual stress, microhardness, and microstructure during the grinding of AerMet100 with white alumina and CBN grinding wheels. The findings indicate that the grinding heat primarily influences the ground surface, whereas the grinding subsurface is significantly impacted by the plastic tensile or compression effects of the grinding force. A study focused on the optimization of both static and dynamic performance in surface grinder machines has been conducted in [13]. This was achieved through an evaluation of their structural integrity and dynamics utilizing finite element analysis. Modal and static studies are conducted using various tool post and column configurations to replicate real-world machining conditions. The modal analysis clarifies the natural frequencies that influence the machine's structure, assisting in the reduction of resonance during machining and enhancing machining precision. Investigation revealed significant distortion at the interface of the grinding stone and primary tool, with a peak deformation of 18.5 μm. The investigation focused on the maximum stretching in machine tool structures across various configurations, leading to enhancements in the structural properties and stability of surface grinding machines. A study on kinematic simulations to predict the extent of surface roughness resulting from grinding was utilized in [14]. The research investigated three specific geometries of abrasive grains (sphere, truncated cone, and cone) alongside a model of single-point diamond dressing. The proposed surface roughness model was empirically validated, revealing a deviation of 7-11 percent. F. An investigation into the

parameters influencing the reduction of cutting temperature during grinding, aiming to establish efficient technological processes for grinding hard materials was performed, [15]. A theoretical solution was derived, with the primary parameter being the maximum cutting temperature resulting from the heating of the formed chips. The maximum cutting temperature has been determined to be significantly higher than the melting point of the machined material. The calculations demonstrated an enhancement in machining productivity through the maintenance of a relatively low grinding temperature and the implementation of multi-pass grinding at a comparatively high workpiece speed. A process for gear grinding utilizing depth grinding with a highly porous abrasive wheel has been developed effectively. This enabled a reduction in energy consumption during processing and an increase in productivity by up to 5 times.

This work introduces the findings of an MCDM analysis performed on the internal grinding processes of SKD11 steel components. To improve the efficiency of the dressing process, it is essential to split this process into three distinct phases: rough dressing, fine dressing, and non-feeding dressing. Therefore, in this experiment, six dressing factors (a_r, n_r, a_f, n_f, and n_0) were investigated. Three objectives were analyzed: minimum SR, minimum MRR, and maximum Lw. The WASPAS method had been used to deal with the MCDM issue, while the MEREC technique was utilized to figure out the criteria weights. The results of the study identified the optimal input parameters for the concurrent minimization of SR, maximization of MRR, and maximization of Lw.

II. Methodology

A. WASPAS method

This study employed the WASPAS technique to tackle the MCDM issue. Adhere to the subsequent steps [16] to implement this method:

Step 1: Create the first decision-making matrix:

$$X = \begin{bmatrix} r_{11} & \cdots & r_{1j} & \cdots & r_{1n} \\ \vdots & \ddots & \vdots & \ddots & \vdots \\ r_1 & \cdots & r_{ij} & \cdots & r_{in} \\ \vdots & \ddots & \vdots & \ddots & \vdots \\ r_{m1} & \cdots & r_{mj} & \cdots & r_{mn} \end{bmatrix}_{m\times n} \quad (1)$$

In which, m and n are the option and criterion number number.

Step 2: Determine the decision matrix's normalized numbers by:

$$r_{ij}^* = \frac{r_{ij}}{\max\limits_i r_{ij}} \quad (2)$$

$$r_{ij}^* = \frac{\min\limits_i r_{ij}}{r_{ij}} \quad (3)$$

where (2) is used for MRR and Lw objectives and (3) is used for Lw.

Step 3: Find the additive significance of options:

$$A_i = \sum_{j=1}^{n} r_{ij}^* \cdot w_j \quad (4)$$

with w_j is the weight of criterion j; i=1÷m.

Step 4: Calculate the multiplicative relative relevance of each alternative:

$$M_i = \prod_{j=1}^{n} \left(r_{ij}^*\right)^{w_j} \quad (5)$$

Step 5: Compute the joint generalized criterion Qi by:

$$Q_i = \lambda \cdot A_i + (1-\lambda) \cdot M_i \quad (6)$$

Step 6: Rank the alternatives by maximizing Qi.

B. MEREC method

This study utilized the MEREC method to determine the weights of the criterion involved. The steps detailed below can be employed to execute this method, [17].

+) Make the initial decision-making matrix:

$$X = \begin{bmatrix} x_{11} & \cdots & x_{1n} \\ x_{21} & \cdots & x_{2n} \\ \vdots & \cdots & \vdots \\ x_{mn} & \cdots & x_{mn} \end{bmatrix} \quad (7)$$

In which, m and n are the number of alternatives and criteria.

+) Compute the value of the normalized matrix by:

- For MRR and Lw targets:

$$h_{ij} = \frac{min\, x_{ij}}{x_{ij}} \quad (8)$$

- For SR target:

$$h_{ij} = \frac{x_{ij}}{max\, x_{ij}} \quad (9)$$

+) Determine the effectiveness of the options Si by:

$$S_i = ln\left[1 + \left(\frac{1}{n}\sum_j \left|ln\left(h_{ij}\right)\right|\right)\right] \quad (10)$$

+) Calculate the efficiency of the ith option S'_{ij} by:

$$S'_{ij} = Ln\left[1 + \left(\frac{1}{n}\sum_{k,k\neq j}\left|ln\left(h_{ij}\right)\right|\right)\right] \quad (11)$$

+) Compute the removal effect of the jth criterion E_j:

$$E_j = \sum_i \left|S'_{ij} - S_i\right| \quad (12)$$

+) Find the weight of criteria by:

$$w_j = \frac{\varepsilon_j}{\sum_k \varepsilon_k} \quad (13)$$

III. Experimental Work

This study generated the input data for the MCDM problem through experimentation. The experiment was structured using the Taguchi technique using an L16 ($4^4 + 2^2$) layout. Table I presents the input parameters together with the levels for each of them. Figure 1 describes the experimental setup which includes the subsequent devices: A MACHT-701 (Japan) grinding machine; SKD11 tool steel workpieces measuring ϕ25 ×ϕ36 × 22 (mm) with a hardness of 58-60 HRC; grinding wheels of 19A 120L 8 ASI T S 1A (Japan) with dimensions of 23×25×8 mm; Mitutoyo SV-3100 surface roughness tester; diamond dresser DKB3E002110; and Caltex Aquatex 3180 oil.

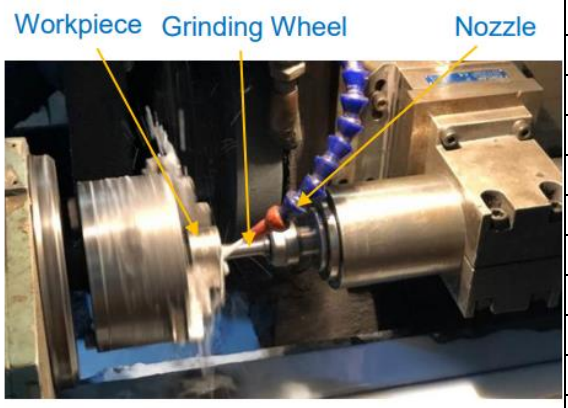

Fig. 1. Experimental setup

Table I. Input factors

No.	Input factors	Code	Unit	Levels			
				1	2	3	4
1	Coarse dressing depth	a_r	mm	0.03	0.04	-	-
2	Coarse dressing times	n_r	times	1	2	3	4
3	Fine dressing depth	a_f	mm	0.005	0.01	0.015	0.02
4	Fine dressing times	n_f	times	0	1	2	3
5	Non-feeding dressing	n_0	times	0	1	2	3
6	Dressing feed rate	S_d	m/min	1	1.5	-	-

The experiment was conducted as follows: The SR of each sample was assessed using surface roughness measurement equipment. To determine Lw and MRR, each sample was ground until the SR surpassed 0.4 (μm). The processing duration for each sample was documented during the experiment to establish Lw. The diameter of each sample was measured before and after each run to calculate the MRR by:

$$MRR_i = \frac{\pi \cdot \left(d_{pbi}^2 - d_{pai}^2\right) \cdot l_{pi}}{4 \cdot T_{wi}} \quad (14)$$

where d_{pbi} and d_{pai} are the inner diameter of sample i before and after grinding (mm); l_{pi} is the length of workpiece i (mm); L_{wi} is the wheel life (min.).

Table II describes the plan and the findings (SR, MRR, and Lw) of the experiment.

Table II. Experimental plan and output findings

N	a_f	n_f	n_0	n_r	a_r	S_d	Ra (μm)	MRR (mm3/s)	Lw (min.)
1	0.005	0	0	1	0.03	1	0.365	0.919	11.267
2	0.005	1	1	2	0.03	1.5	0.214	1.041	12.733
3	0.005	2	2	3	0.04	1	0.195	1.122	12.697
4	0.005	3	3	4	0.04	1.5	0.242	1.111	11.423
5	0.01	0	1	3	0.04	1.5	0.185	1.246	11.803
6	0.01	1	0	4	0.04	1	0.248	1.267	12.430
7	0.01	2	3	1	0.03	1.5	0.252	1.178	11.147
8	0.01	3	2	2	0.03	1	0.217	1.225	12.077
9	0.015	0	2	4	0.03	1.5	0.306	1.488	12.547
10	0.015	1	3	3	0.03	1	0.324	1.372	12.077
11	0.015	2	0	2	0.04	1.5	0.341	1.271	12.027
12	0.015	3	1	1	0.04	1	0.354	1.199	12.503
13	0.02	0	3	2	0.04	1	0.318	1.227	12.177
14	0.02	1	2	1	0.04	1.5	0.313	1.265	10.620
15	0.02	2	1	4	0.03	1	0.326	1.125	13.153
16	0.02	3	0	3	0.03	1.5	0.363	1.190	12.230

IV. Calculating Best Input Factors

After finishing the experiment, the SR, MRR, and Tw values will serve as input variables for the MCDM problem. The MEREC approach, provided in Section 2.2, was employed to determine the weights for the criterion as follows: The values hj received normalization through the application of equations (8) and (9). The values of Si and Sij' were obtained from equations (10) and (11). Equation (12) has been used to assess the effects of eliminating the criterion. The criterion weights were calculated using Equation (13), which delineates them. The weights assigned to SR, MRR, and Lw were 0.4076, 0.4042, and 0.1882, respectively, as determined through calculations.

``Section 2.1 outlines the implementation of the WASPAS approach. Following the establishment of the initial decision-making matrix, the normalized values of the decision matrix, denoted as r_{ij}^*, have been computed using Equations (2) for MRR and Lw, and Equation (3) for SR. Subsequently, the additive significance of each alternative Ai is determined using

Equation (4). Determine the multiplicative relative relevance for each option Mi using the formula (5). After that, determine the joint generalized criterion Qi using equation (6). Finally, sort Qi for ranking options. Table III presents various results from calculations alongside the ranking of alternatives. Figure 2 illustrates the relationship between solutions and Qi. Table III indicates that option 2 is optimal, demonstrating the highest Qi value (Qi=0.7527).

Table III. Calculated results and ranking of options by WASPAS method

Trial	r_{ij}			Qi	Rank
	Ra	MRR	Lw		
1	0.5066	1.6196	0.8566	0.6929	4
2	0.8657	1.4288	0.9681	0.7527	1
3	0.9497	1.3266	0.9653	0.7444	2
4	0.7654	1.3390	0.8685	0.6878	5
5	1.0000	1.1942	0.8974	0.7081	3
6	0.7469	1.1745	0.9450	0.6520	9
7	0.7341	1.2628	0.8474	0.6564	7
8	0.8537	1.2144	0.9181	0.6836	6
9	0.6038	1.0000	0.9539	0.5713	16
10	0.5712	1.0841	0.9181	0.5803	15
11	0.5432	1.1707	0.9143	0.5957	13
12	0.5225	1.2411	0.9506	0.6148	11
13	0.5819	1.2123	0.9258	0.6184	10
14	0.5918	1.1764	0.8074	0.5920	14
15	0.5677	1.3228	1.0000	0.6559	8
16	0.5091	1.2505	0.9298	0.6104	12

Figure 2 displays the ranking of options derived from the WASPAS analysis, based on the data presented in Table III. The results indicate that option 2 is the most favorable choice. According to the analysis and Table II, the best input parameters for simultaneously achieving the minimum SR, maximum MRR, and maximum L_w are as follows: a_r=0.03 (mm); n_r=2 (times); a_f=0.005 (mm); n_f=1 (times); n_0=1; and Sd=1.5 (m/min.).

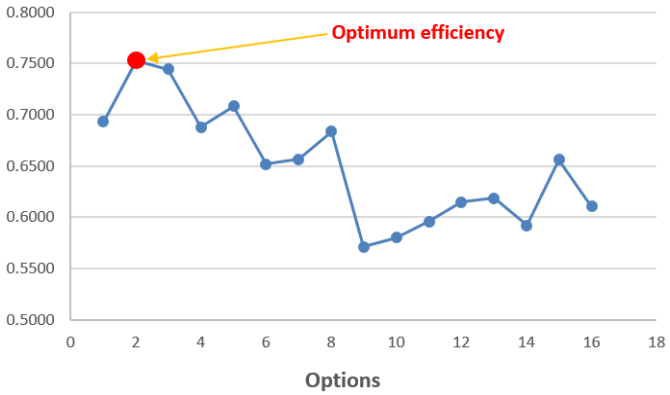

Fig. 2. Ranking of options

V. Conclusion

This work reports the results of an MCDM analysis intended for finding the ideal input elements for the internal grinding of cylindrically shaped components fabricated from SKD11 tool steel. This study investigates three objectives: minimizing SR, maximizing MRR, and maximizing L_w. Furthermore, six input parameters were examined: a_r, n_r, a_f, n_f, n_0, and S_d. The experiment employed the Taguchi technique with an L16 ($4^4 + 2^2$) design, and the results were analyzed utilizing the Minitab R19 software. The MCDM problem has been effectively resolved, and the optimal input parameters were found. The results of the work reveal that the best process factors for achieving the lowest SR, maximum MRR, and maximum Tw concurrently are: a_r=0.03 (mm); n_r=2 (times); a_f=0.005 (mm); n_f=1 (times); n_0=1; and S_d=1.5 (m/min.). Furthermore, the WASPAS approach is capable of addressing MCDM issues in the internal grinding process. The results are obtained from the analysis of internal grinding operations involving SKD11 steel. It may also function as a reference for the analysis of additional material grinding processes.

Acknowledgment

The work has been supported by Thai Nguyen University of Technology.

References

[1] Peng, R., R. Wang, J. Gao, L. Zhao, X. , J. Yao , Improve the grinding performance of Inconel 718 superalloys by using an internal cooling wheel with a phyllotaxy of abrasive arrangement. *The International Journal of Advanced Manufacturing Technology,* 2024. 135(5): p. 2517-2537.

[2] Zhang, S., Z. Zhang, H. Xing, G. Hao, X. Liang , Analysis and optimization of abrasive waterjet dressing parameters for surface texturing of diamond grinding wheels. *Diamond and Related Materials,* 2024: p. 111661.

[3] Denkena, B., H. Klemme, and D. Stoppel, Condition monitoring of grinding wheels: Potential of internal control signals. Production Engineering, 2024: p. 1-11.

[4] Jiang, L., Y. Du, Q. Song, Z. Liu, Q. Luan, H. Wang, C. Cao, Design and application of grooved grinding head for improving the machined surface quality of ceramic composites. *Ceramics International,* 2024. 50(20): p. 37954-37967.

[5] Hu, L., B. Li, L.H. Pueh, Z. Wang, Y. Wang, Effect of single/multi-particle grinding parameters on surface properties of bearing steel GCr15. *Engineering Science and Technology, an International Journal,* 2024. 58: p. 101851.

[6] Irazu, E., U. Alonso, B. Izquierdo, L. Godino , Grinding of C/SiC ceramic matrix composites: Influence of grinding parameters on tool wear. *Wear,* 2024. 558: p. 205582.

[7] Wang, F., S. Xuan, Z. Chang, K. Jin, Y. Gao, H. Wang, Q. Song , Effect of Grinding Parameters on Industrial Robot Grinding of CFRP and Defect Formation Mechanism. *International Journal of Precision Engineering and Manufacturing-Green Technology,* 2024. 11(2): p. 427-438.

[8] Liu, H., H. Han, Q. Jiang, B. Zhang , Mechanisms in the machinability improvement of Inconel 718 superalloy through ultra-high-speed grinding. *Journal of Materials Processing Technology,* 2024. 333: p. 118614.

[9] Jin, G., Y. Gao, P. Huang, J. Zhou, Y. Tang , Surface roughness in grinding outer ring inner raceway of tapered roller bearing. *The International Journal of Advanced Manufacturing Technology,* 2024. 131(5): p. 2447-2463.

[10] Meng, Q., B. Guo, K. Li, G. Wu, H. Zhao, J. Jia, Z. Guo, Q. Zhao, Stability prediction and optimization of multi-regenerative weak stiffness grinding system based on microstructured tool. *Mechanical Systems and Signal Processing,* 2024. 208: p. 111010.

[11] Hu, L., H. Zhang, J. Zha, Y. Chen, Surface topography of cylindrical precision grinding based on multi-source information fusion. *Proceedings of the Institution of Mechanical Engineers, Part E: Journal of Process Mechanical Engineering,* 2024. 238(6): p. 2894-2907.

[12] Xin, H., X. Dong, C. Xian, Q. Cheng, H. Dai, C. Yao, M. Cui, G. Li , Study on the formation of surface affected layer in grinding ultra-high strength steel. *The International Journal of Advanced Manufacturing Technology,* 2024. 135(5): p. 2191-2213.

[13] Hung, L.X., T.N. Giang, Q.. Tran, N.H. Linh, D.N. Nguyen, V.N. Pi , Determining the optimum set of dressing parameters satisfying minimum surface roughness when conducting the internal grinding of hardened SKD11 steel. *Solid State Phenomena,* 2021. 324: p. 58-65.

[14] Liu, Y., A. Warkentin, R. Bauer, Y. Gong , Investigation of different grain shapes and dressing to predict surface roughness in grinding using kinematic simulations. *Precision Engineering,* 2013. 37(3): p. 758-764.

[15] Novikov, F., A. Hutorov, O. Yermolenko, O. Yermolenko, A. Ivashura , Theoretical Justification for Increasing Efficiency of Grinding Technological Processes Based on the Reduction of Cutting Temperature, in *Design, Simulation, Manufacturing: The Innovation Exchange.* 2024, Springer. p. 309-318.

[16] Zavadskas, E.K., J. Antuchevičienė, J. Šaparauskas, Z. Turskis, MCDM methods WASPAS and MULTIMOORA: Verification of robustness of methods when assessing alternative solutions. *Journal of Economic Computation and Economic Cybernetics Studies and Research,* No. 2, Vol. 47, 2013, p. 5-20. -

[17] Keshavarz-Ghorabaee, M., M. Amiri, E. K. Zavadskas, Z. Turskis, J. Antucheviciene, Determination of objective weights using a new method based on the removal effects of criteria (MEREC). *Symmetry,* 2021. 13(4): p. 525.

Contribution of Individual Authors to the Creation of a Scientific Article (Ghostwriting Policy)

A.The design and analysis of the experiment were done by Luu Anh Tung and Nguyen Thanh Tu. Nguyen Thanh Tu worked with Vu Duc Binh and Le Duc Bao to draft the manuscript. Every author examined, discussed about, and offered valuable criticism on the manuscript's content. It was Nguyen Thanh Tu and Dinh Van Thanh who revised the paper. Lastly, the published version of the work has been read, approved, and agreed upon by all authors.

Sources of Funding for Research Presented in a Scientific Article or Scientific Article Itself

No funding was received for conducting this study.

Conflict of Interest

The authors have no conflicts of interest to declare.

Creative Commons Attribution License 4.0 (Attribution 4.0 International, CC BY 4.0)

This article is published under the terms of the Creative Commons Attribution License 4.0
https://creativecommons.org/licenses/by/4.0/deed.en_US